

Seismic quiescence and activation prior to the 2025 *M*8.8 Kamchatka, Russia earthquake

K. Z. Nanjo^{1,2,3,4,†}, J. Yazbeck⁵, I. T. Baughman⁵, and J. B. Rundle^{5,6,7}

¹Global Center for Asian and Regional Research, University of Shizuoka, Shizuoka, Japan

²Center for Integrated Research and Education of Natural Hazards, Shizuoka University, Shizuoka, Japan

³Institute of Statistical Mathematics, Tokyo, Japan

⁴Japan Agency for Marine-Earth Science and Technology, Yokohama Institute for Earth Sciences, Yokohama, Japan

⁵Department of Physics and Astronomy, University of California, Davis, CA, USA.

⁵Department of Earth and Planetary Sciences, University of California, Davis, CA, USA.

⁷Santa Fe Institute, Fe, NM, USA.

Corresponding author: K. Z. Nanjo (nanjo@u-shizuoka-ken.ac.jp)

†Now at Department of Physics and Astronomy, University of California, Davis, CA, USA.

ORCID: <https://orcid.org/0000-0003-2867-9185> (K.Z.N), <https://orcid.org/0000-0003-0223-5260> (J.Y.), [0009-0005-7895-3084](https://orcid.org/0009-0005-7895-3084) (I.T.B), <https://orcid.org/0000-0002-1966-4144> (J.B.R.).

Key Points:

- ETAS modeling identified about 20 years of seismic quiescence before the 2025 *M*8.8 Kamchatka mainshock
- A sharp activation began about 10 days before the mainshock, coincident with an *M*7.4 foreshock

- Similar quiescence–activation patterns before the 1997 $M7.8$ and 2006 $M8.3$ events suggest a recurring precursor in this region

Abstract

The 29 July 2025 Kamchatka earthquake, of magnitude $M8.8$, provides a unique opportunity to investigate the preparatory processes of a great subduction event. Despite Kamchatka's high seismic activity, the long-term evolution of seismicity preceding major ruptures has been poorly documented. Identifying temporal patterns—such as multiyear quiescence and short-term activation—is essential for understanding megathrust failure processes. We applied the Epidemic-Type Aftershock Sequence (ETAS) model and change-point analysis to earthquakes with $M \geq 5$ within a 100-km radius of the 2025 mainshock epicenter, using the Advanced National Seismic System (ANSS) catalog spanning 1975–2025. This approach quantified temporal variations in the seismicity rate and detected statistically significant change points. We identified a pronounced approximately 20-year quiescent interval beginning around mid-2003, followed by an abrupt activation that commenced with the $M7.4$ foreshock on 20 July 2025. A similar quiescence-to-activation sequence near the eventual hypocenter was also observed for the 1997 $M7.8$ Kronotsky and 2006 $M8.3$ Simushirskoe earthquakes, which ruptured segments immediately north and south of the 2025 rupture, respectively. These results suggest that heightened seismic activity following multiyear quiescence is a recurrent feature of the Kamchatka–Kuril subduction system hosting large megathrust earthquakes.

Plain Language Summary

On July 29, 2025, a magnitude 8.8 earthquake struck Russia's Kamchatka Peninsula. We examined nearly 50 years of earthquake records to see how activity changed leading up to this event. We found a long quiet spell—about 20 years starting around 2003—followed by a sharp increase in earthquakes about 10 days before the mainshock, including a magnitude 7.4 foreshock. A similar “quiet-then-active” pattern also appeared before nearby major earthquakes in 1997 and 2006. These repeating patterns suggest that, in the Kamchatka subduction zone, periods of low activity followed by activation can be part of the build-up to great earthquakes. While this does not enable exact prediction, tracking such changes could improve how near-term earthquake risk is assessed.

1 Introduction

Large subduction earthquakes around the Pacific Rim have repeatedly generated devastating tsunamis and significant crustal deformation, providing key case studies for understanding the preparatory processes of megathrust events. The Kamchatka Peninsula, at the northwestern edge of the Pacific subduction zone, is among the most seismically active regions on Earth, where the Pacific Plate subducts beneath the North American Plate at about 8 cm yr⁻¹ (USGS, 2025), where USGS represents the United States Geological Survey. Historical records show multiple events with magnitudes $M \geq 8$, including the 1952 Kamchatka $M9.0$ earthquake that produced a trans-Pacific tsunami (Fig. 1a). Despite this long history, the temporal evolution of seismicity preceding such large events remains poorly documented.

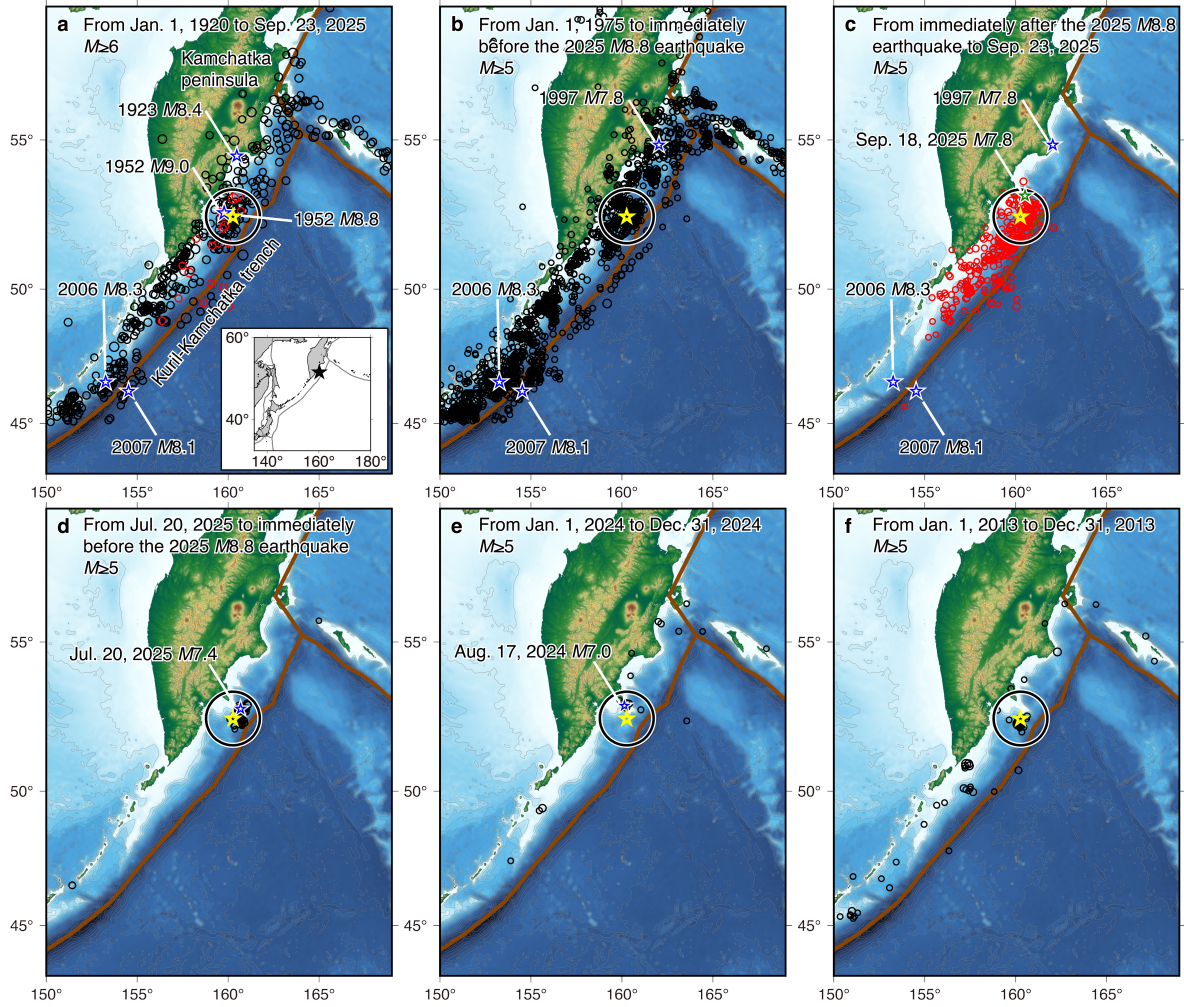


Figure 1. Spatial distribution of earthquakes. **(a)** Earthquakes with $M \geq 6$ (depth ≤ 100 km) from Jan. 1, 1920 up to, but not including, the 2025 $M8.8$ mainshock (black), and from immediately after the mainshock through Sep. 23, 2025 (red). Plate boundaries from Bird (2003) are shown as red curves. The yellow star marks the 2025 $M8.8$ epicenter. Blue stars mark events of $M \geq 8$. The black circle (100-km radius centered on the $M8.8$ epicenter) delineates the analysis window used in Figs. 2–6. Inset shows the epicenter (star) of the 2025 $M8.8$ epicenter. **(b)** Same as **(a)**, but for $M \geq 5$ earthquakes since Jan. 1, 1975 (black). Blue stars mark events with $M \geq 7.8$. **(c)** Same as **(b)**, but for the period from immediately after the 2025 $M8.8$ mainshock to Sep. 23, 2025. The green star marks the Sep. 18, 2025 $M7.8$ event. **(d)** Same as **(b)**, but for Jul. 20, 2025 up to, but not including, the 2025 $M8.8$ mainshock. The blue star marks the July 20, 2025 $M7.4$

foreshock. (e) Same as (b), but for Jan. 1–Dec. 31, 2024. The blue star marks the Aug. 17, 2024 *M*7.0 event. (f) Same as (b), but for Jan. 1–Dec. 31, 2013.

On 29 July 2025, an *M*8.8 earthquake occurred off eastern Kamchatka (Fig. 1). The event produced strong shaking and a moderate tsunami, and drew global attention because it ruptured a segment that had been relatively quiet for more than a decade. To investigate its source processes, we analyzed temporal variations in seismicity within a 100-km radius of the 2025 epicenter.

Our analysis reveals a pronounced period of seismic quiescence beginning around 2003 and lasting for about two decades prior to the mainshock. Notably, around 10 days before the *M*8.8 event, an *M*7.4 earthquake struck the same area. Local seismicity then increased markedly, suggesting that the *M*7.4 shock may have acted as a trigger, promoting failure on the locked portion of the megathrust.

Comparable precursory patterns—quiescence followed by foreshock activation—have been reported for other great earthquakes, including the 1997 *M*7.8 Kronotsky, Kamchatka event (Soloviev, 2011, 2020), the 2004 *M*9.0 Sumatra event (e.g., Mignan et al., 2006; Soloviev & Lyubushin, 2007; Imoto & Yamamoto, 2008; Katsumata, 2015; Soloviev, 2020), the 2006 *M*8.3 Simushirskoe, Kuril event (Soloviev, 2011, 2020; Katsumata & Zhuang, 2020), the 2010 *M*6.4 Jiashian, Taiwan earthquake (Wen et al., 2016), and the 2011 Tohoku event (e.g., Katsumata, 2011, 2017; Kato et al., 2012; Nanjo et al., 2012; Nagao et al., 2014; Ogata, 2016).

The 2025 Kamchatka sequence nonetheless provides new insight owing to its clear spatial confinement and the availability of continuous instrumental data spanning more than five decades. Recognizing such patterns is crucial for advancing our understanding of the physics of the earthquake cycle and for improving probabilistic assessments of megathrust occurrence.

In this study, we present a detailed analysis of the temporal evolution of seismicity prior to the 2025 *M*8.8 Kamchatka earthquake. We quantify the long-term quiescence and examine the subsequent activation following the *M*7.4 foreshock. Our results add to growing evidence

that temporal variations in seismicity can illuminate the preparatory stages of great earthquakes.

2 Materials and Methods

Large earthquakes are often preceded by a period of seismic quiescence—that is, a pronounced, multi-year reduction in regional seismicity (Katsumata and Nakatani, 2021). Recognized as a potential intermediate-term earthquake precursor (e.g., Scholz, 2019), quiescence has been studied for decades. Early reports (e.g., Inouye, 1965; Utsu, 1968; Mogi, 1969; Ohtake et al., 1977; Kanamori, 1981) generally lacked an objective definition, whereas later work introduced quantitative metrics, including ZMAP (Wiemer & Wyss, 1994; Katsumata, 2011, 2017), ETAS (Epidemic-Type Aftershock Sequence) modeling (Ogata, 1999), and the RTL/RTM approach (e.g., Sobolev & Tyupkin, 1997; Nagao et al., 2011). Collectively, these advances have established seismic quiescence as an objectively quantifiable anomaly that can precede large earthquakes by years to decades.

Sobolev (2020) proposed that large earthquakes are often preceded by a phase of seismic activation—that is, a marked increase in regional seismicity following a period of quiescence. The duration of activation ranges from several days to many months. Sobolev (2020) defined the interval between the end of quiescence and the mainshock as the foreshock-activation phase. In its final stage, events may occur whose locations coincide with the subsequent mainshock source.

Metrics developed to quantify quiescence can likewise be used to characterize activation. Here we adopt the ETAS model (Ogata, 1999), which explicitly represents triggered seismicity and therefore does not require preprocessing declustering, unlike ZMAP or RTL/RTM. Conclusions can be sensitive to the choice of declustering parameters (Wang et al., 2010), so ETAS offers a more self-consistent framework. Before introducing ETAS, we briefly review the Omori–Utsu (OU) law (Utsu, 1961), as follows.

Aftershock rates commonly follow the OU law (Utsu, 1961), $\lambda_{OU}(t)=k(c+t)^{-p}$, where $\lambda_{OU}(t)$ is the conditional intensity (occurrence rate) at time t for events with $M \geq M_{th}$, and $k > 0$, $c > 0$, and $p > 0$. The case $p=1$ reduces to the original Omori (1894) form and is consistent with rate-and-

state friction theory (Dieterich, 1994). Values of $p < 1$ and $p > 1$ correspond to slower and faster temporal decay, respectively. The ETAS model described below represents an earthquake sequence as the superposition of OU-type decays triggered by each prior event.

In the ETAS framework (Ogata, 1999), seismicity is decomposed into a homogeneous Poisson background and a triggered (clustered) component. Each event with magnitude M_i ($\geq M_{th}$) at time t_i ($< t$) contributes $v_i(t) = K_0 \exp\{\alpha(M_i - M_{th})\}(t - t_i + c)^{-p}$ so that the total rate at time t given the history $H_t = \{(t_i, M_i): t_i < t\}$ is $\lambda(t|H_t) = \mu + \sum_{t_i < t} v_i(t)$, where $\mu > 0$ is the background rate. The parameter vector $\theta = (\mu, K_0, \alpha, c, p)$ characterizes the sequence; units are μ in day^{-1} , c in days, α and p dimensionless, and K_0 having units day^{p-1} so that v_i has units of a rate. Parameters are estimated by maximum likelihood, and model comparison uses the Akaike Information Criterion (AIC; Akaike, 1974). Because K_0 depends on M in the model, it is necessary to assume a magnitude at which a value for K_0 needs to be known. Throughout this study, $M=9.0$ was assumed for estimating K_0 .

Goodness of fit can be visualized by comparing observed and model-based cumulative counts in ordinary time and via time-rescaling diagnostics (Ogata & Tsuruoka, 2016). One can visualize this comparison in two types of graphs: one graph using ordinary time and the other using transformed time. Here, transformed time is converted from ordinary time in such a way that the transformed sequence follows the Poisson process (uniformly distributed occurrence times) with unit intensity (occurrence rate). When a good approximation of observed seismicity is presented by the model, one observes an overlap between the observation rate and model rate in both types of graphs.

We performed change-point analysis using ETAS and AIC (Ogata & Tsuruoka, 2016; Akaike, 1974), following Kumazawa et al. (2010, 2019). We define $\Delta\text{AIC} = \text{AIC}_{\text{single}} - \text{AIC}_{\text{2stage}}$, where $\text{AIC}_{\text{single}}$ is AIC for the standard (single-stage) ETAS that uses time-invariant parameters and $\text{AIC}_{\text{2stage}}$ is the AIC for the two-stage ETAS that allows parameters to differ before and after a change time T_c (both fitted to events with $M \geq M_{th}$; see Nanjo et al., 2023; 2025a,b). The two-stage ETAS is better fitted to the data than the single-stage ETAS model and candidate change is flagged if $\Delta\text{AIC} \geq 2q$ at T_c , where q is the degree of freedom associated with scanning T_c (Ogata,

1992; Kumazawa et al., 2010). q depends on sample size (number of earthquakes) (Ogata, 1992; Kumazawa et al., 2010). Given $\Delta\text{AIC} \geq 2q$, a 68% confidence interval for T_c is obtained (Kumazawa et al., 2010). To calculate it, we considered the likelihood of the two-stage ETAS model, $\exp\{-(\text{AIC}_{2\text{stage}} + 2q)/2\}$ for different T_c -values. The normalization of the likelihoods for all T_c -values assigned a probability mass, and the central 68% of this mass provided a change point's confidence interval.

3 Data

We used the Advanced National Seismic System (ANSS; USGS, 2017) earthquake catalog (<https://earthquake.usgs.gov/earthquakes/search/>, downloaded on Sep. 25, 2025), which provides source parameters (e.g., hypocenters, magnitudes, phase picks, and amplitudes). From this catalog, we extracted events of $M \geq 5$ with a complete hypocenter and origin-time information occurring between 1920 and Sep. 23, 2025, within 150–169°E, 43–59°N, and depths of 0–100 km. For Fig. 1a, we set a minimum magnitude of $M=6$ to mitigate temporal completeness issues and ensure homogeneity over the full 1920–2025 span.

According to USGS (2025), the Jul. 29, 2025 $M8.8$ event was the latest in a sequence offshore the Kamchatka Peninsula that began 10 days earlier and included an $M7.4$ earthquake on Jul. 20, 2025. As of Jul. 30, 2025, 24 aftershocks of $M \geq 5$ had been recorded, including $M6.9$ and $M6.3$ events (USGS, 2025).

The magnitude–time (M – t) plots in the bottom panels of Fig. 2 confirm this sequence (USGS, 2025). We identified 48 earthquakes of $M \geq 5$ (depth 0–100 km) between Jul. 20, 2025 and immediately before the Jul. 29, 2025 $M8.8$ event within a 100-km radius of the eventual epicenter (Fig. 1d). After the $M8.8$ mainshock, 150 earthquakes of $M \geq 5$ occurred, including an $M7.8$ event on Sep. 18, 2025 (Fig. 1c). Prior to the Jul. 20, 2025 $M7.4$ event, notable activity since 1975 includes the Aug. 17, 2024 $M7.0$ event (Fig. 1e) and an earthquake swarm with M up to 6.1 during May 19–21, 2013 (Fig. 1f).

4 Results

Figure 2 shows ETAS fits to earthquakes with $M \geq 5$ ($M_{th}=5$) from Jan. 1, 1975 to Sep. 23, 2025, within a 100-km radius of the eventual $M8.8$ epicenter. The panels compare the observed occurrence rate (black) with the ETAS rate (red) and reveal a sustained deviation followed by a return to baseline prior to the $M8.8$ mainshock. Following Ogata & Tsuruoka (2016) and Kumazawa et al. (2019), we used two time intervals: a target interval, over which the parameter θ was estimated, and a preceding precursory interval to account for long-memory effects of earlier events implied by the OU kernel. Letting “day 0” denotes 00:00:00 on Jan. 1, 1975, we set the precursory and target intervals to 0– S and S – T , respectively, with $S=0.01$ days (Jan. 1, 1975 00:14:25) and $T=18528.72$ days (Sep. 23, 2025 17:15:22, the last event in the analyzed earthquakes).

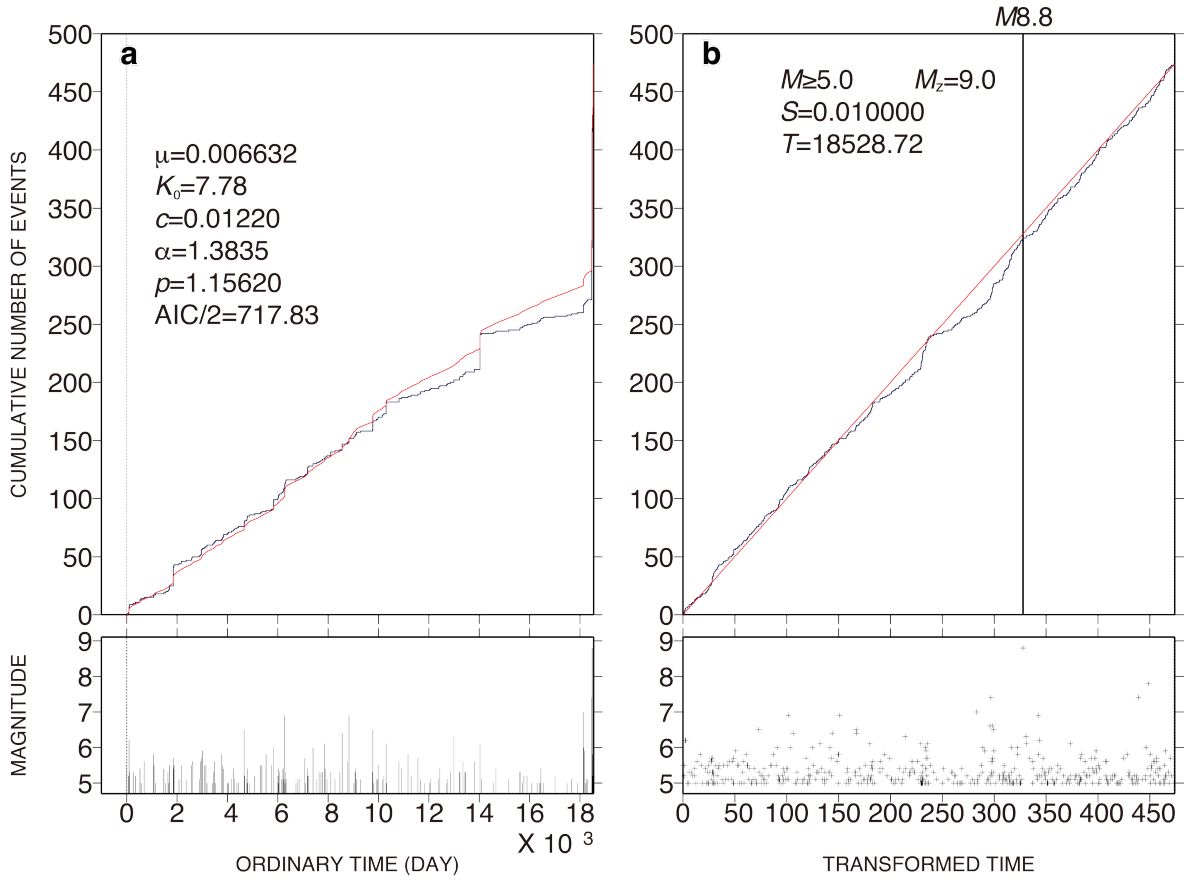


Figure 2. ETAS modeling over the full study window. **(a)** Cumulative count of earthquakes with $M \geq 5$ ($M_{th}=5$) within a 100-km radius of the $M8.8$ epicenter (large black circle in Fig. 1) as a function of ordinary time. The ETAS-based cumulative curve (red) is fitted to the observations (black) over the target interval from Jan. 1, 1975 to Sep. 23, 2025. Day 0 is Jan. 1, 1975 00:00:00, $S=0.01$ days (Jan. 1, 1975 00:14:25, vertical dashed line), and $T=18528.72$ days (Sep. 23, 2025 17:15:22, the last event in the analyzed earthquakes). The small panel below shows the magnitude–time ($M-t$) diagram for the same data. **(b)** Same as **(a)**, but plotted in transformed time. See the Materials and Methods section for explanation of transformed time.

The deviation and subsequent return are more apparent in transformed time (Fig. 2b) than in ordinary time (Fig. 2a). The deviation begins between 10,000 and 11,000 days (May 19, 2002–Feb. 12, 2005), and the return initiates around the $M7.0$ event in 2024 and the $M7.4$ event on July 20, 2025. These features are consistent with a phase of seismic quiescence followed by activation prior to the $M8.8$ mainshock.

To identify the most probable onset of quiescence, we performed change-point analysis (Fig. 3). We scanned candidate change times T_c over Jan. 1, 1990 to Jan. 1, 2010 (in days since Jan. 1, 1975), fitting both the two-stage and single-stage ETAS models to events from Jan. 1, 1975 up to, but not including, the 2025 $M7.4$ event. Instances with $\Delta AIC \geq 2q$ indicate the two-stage model fits better. The 68% confidence interval for the change point (blue band) is $T_c=10,100$ – $12,100$ days (Aug. 27, 2002–Feb. 17, 2008). ΔAIC values were mostly below $2q$ and increasing before $T_c \approx 10,100$ days. These values remained above $2q$, and were roughly stable thereafter. A smoothing discontinuity appears near the lower bound of the interval. Considering that the maximum ΔAIC occurs at $T_c=10,400$ days (Jun. 23, 2003; red circle in Fig. 3), we regard $T_c=10,400$ days as the most probable onset of quiescence.

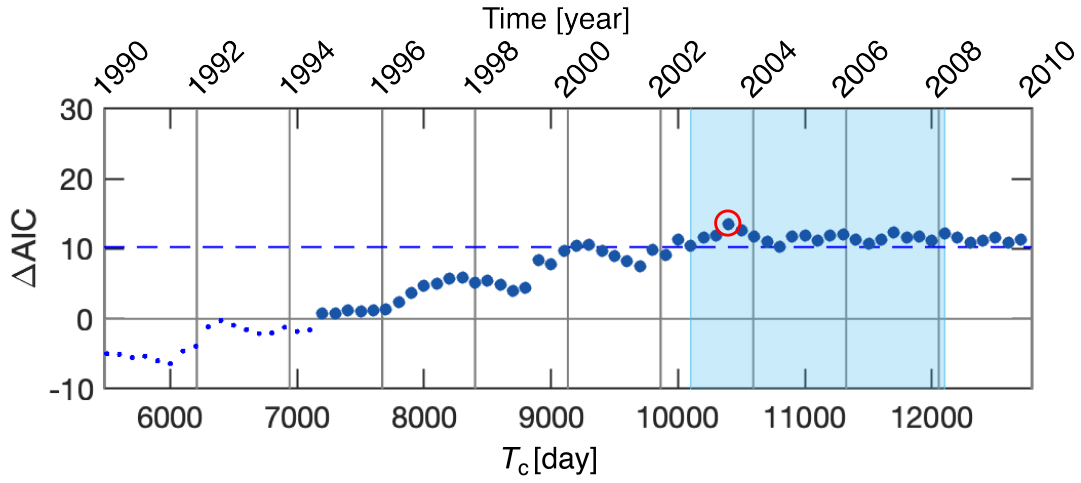


Figure 3. ΔAIC as a function of the candidate change time T_c scanned over Jan. 1, 1990–Jan. 1, 2010 (in days since Jan. 1, 1975). The two-stage and standard (single-stage) ETAS models are fitted to events with $M \geq 5$ ($M_{\text{th}}=5$) from Jan. 1, 1975 up to, but not including the $M7.4$ foreshock. The red circle marks $T_c=10,400$ days, which is adopted as T in Fig. 4. In some cases, the two-stage optimization did not fully converge; when a ΔAIC value was nevertheless returned for that T_c , it is plotted as a small dot. The blue band ($T_c=10,100$ – $12,100$ days; Aug. 27, 2002–Feb. 17, 2008) denotes the 68% confidence interval for the change point. Thin vertical ticks indicate Jan. 1 of 1990, 1992, ..., 2010. The horizontal dashed line shows the $2q$ threshold. The horizontal solid line indicates $\Delta\text{AIC}=0$.

Figure 4 further corroborates quiescence using three intervals: precursory $0-S=0.01$ days (Jan. 1, 1975 00:00:00–00:14:25), target $S-T$ ($=T_c=10,400$ days) (through Jun. 23, 2003 00:00:00), and prediction $T-T_{\text{end}}$ ($=18,417.61$ days=June 4, 2025 14:39:36; the last event before the $M7.4$ foreshock). We extrapolated the ETAS rate through the prediction interval using θ estimated over the target interval and compared it with observations. The observed cumulative curve generally tracks the lower boundary of the 95% confidence envelope (parabolic bounds). A swarm with M up to 6.1 during May 19–21, 2013 (Fig. 1f) temporarily elevated the rate, but after the swarm ceased, the cumulative curve approached the envelope’s lower boundary asymptotically.

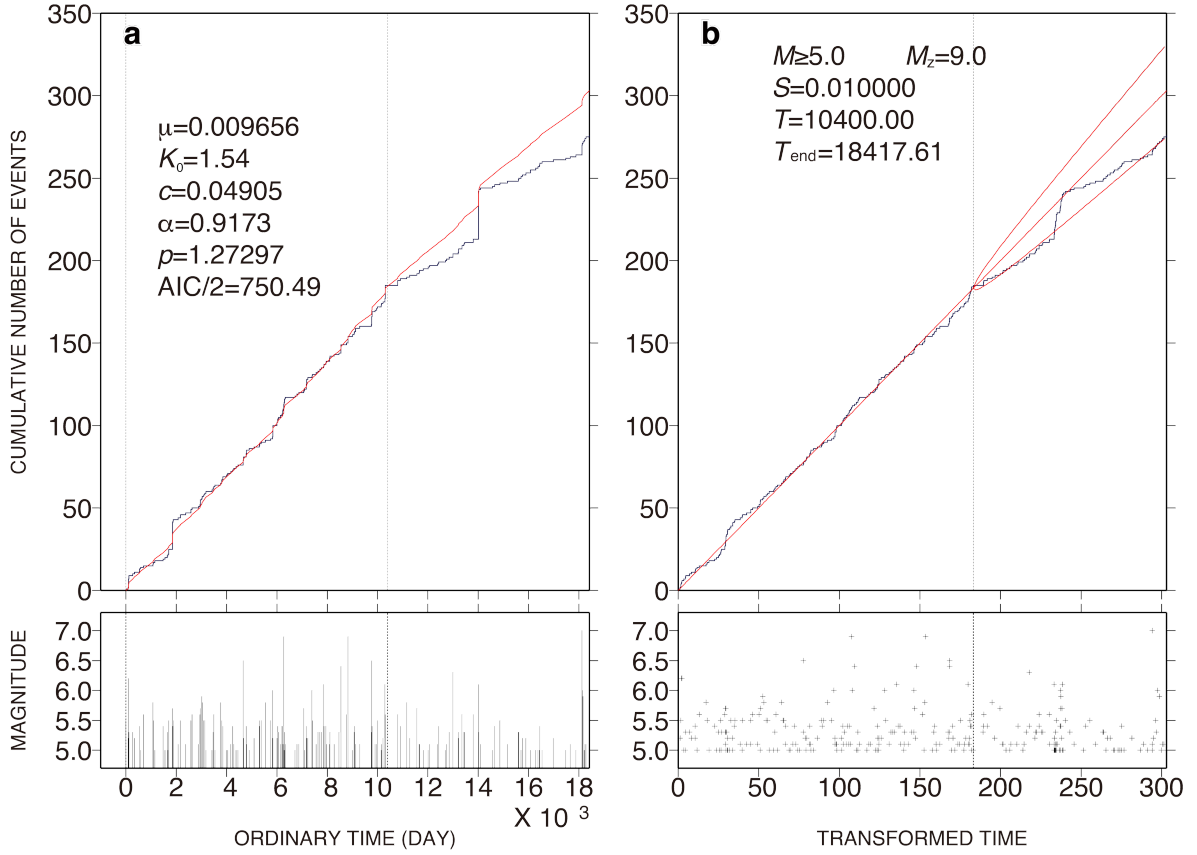


Figure 4. Seismic quiescence diagnosed by ETAS modeling for $M \geq 5$ ($M_{\text{th}}=5$) earthquakes within a 100-km radius of the $M_{8.8}$ epicenter. **(a)** Cumulative counts (black) and ETAS fit (red) over the target interval from $S=0.01$ days (Jan. 1, 1975 00:14:25, first vertical dashed line) to $T=10,400$ days (Jun. 23, 2003 00:00:00, second vertical dashed line) plotted in ordinary time, with the ETAS curve extrapolated through the prediction interval ($T-T_{\text{end}}$) up to immediately before the Jul. 20, 2025 $M_{7.4}$ foreshock, where $T_{\text{end}}=18,417.61$ days (the last event before the $M_{7.4}$ foreshock). **(b)** Same as **(a)**, but in transformed time; the vertical dashed line marks June 23, 2003. The parabolic envelope denotes the 95% confidence bounds for the ETAS extrapolation.

Because visual inspection of Fig. 2 does not uniquely identify the onset of activation—although times around the 2024 $M_{7.0}$ and July 20, 2025 $M_{7.4}$ events are plausible—we applied the same change-point procedure for activation (Fig. 5). Here we analyzed the period from Jan. 1, 2014 up to, but not including the $M_{8.8}$ mainshock, and found that stable evaluation of

AIC_{2stage} for all candidate T_c necessitated reducing the number of free parameters. We therefore fixed $\alpha=1.27$ (as estimated in Fig. 4), holding it common to both subperiods (independent of T_c). Given this predefined α , we optimized (μ, K_0, c, p) separately on each side of T_c to compute AIC_1 and AIC_2 , with $AIC_{2stage} (=AIC_1+AIC_2)$. For comparison, we also computed AIC_{single} for the single-stage ETAS model under the same constraint ($\alpha=1.27$) by optimizing (μ, K_0, c, p) over the full interval.

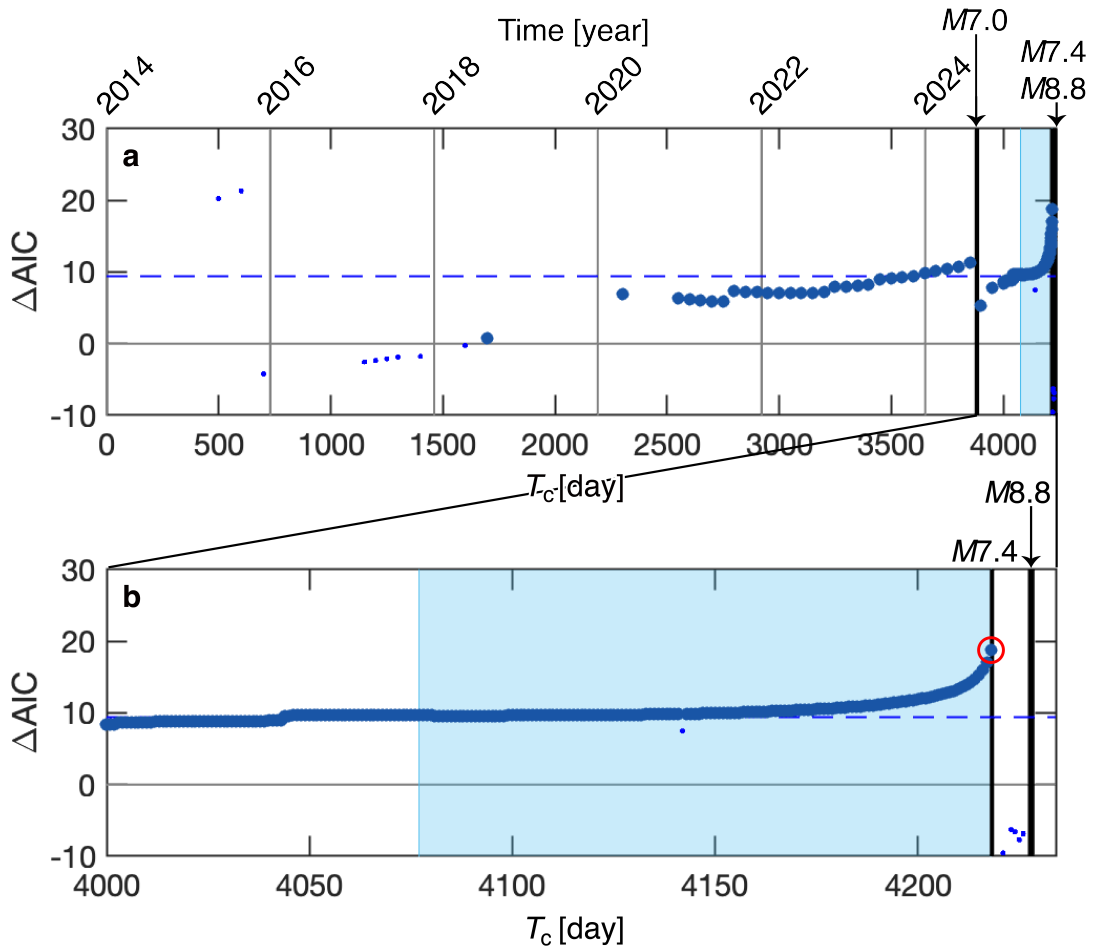


Figure 5. Same as Fig. 3, but for Jan. 1, 2014 to immediately before the $M8.8$ mainshock. The two-stage and standard (single-stage) ETAS models are fitted to events with $M \geq 5$ ($M_{th}=5$) from Jan. 1, 2014 up to, but not including, the $M8.8$ mainshock. (a) ΔAIC versus candidate change point time $T_c=0-4,234$ days (days since Jan. 1, 2014; i.e., Jan. 1, 2014–Aug. 5, 2025). The blue band $T_c=4,077-4,218$ days (Mar. 1, 2025–Jul. 20, 2025) denotes the 68% confidence interval for

the change point. Stable evaluation of AIC_{2stage} across all T_c was difficult, so we fixed $\alpha=1.27$ (from Fig. 4), independent of T_c , and optimized (μ, K_0, α, c) separately before and after each T_c to obtain AIC_1 and AIC_2 , with $AIC_{2stage}=AIC_1+AIC_2$. The single-stage AIC_{single} was computed under the same constraint ($\alpha=1.27$) by optimizing (μ, K_0, α, c) over the full interval, and $\Delta AIC = AIC_{single} - AIC_{2stage}$. **(b)** Same as **(a)**, but zoomed for $T_c \geq 4000$ days (since Dec 12, 2024). The red circle marks $T_c=4218$ days (Jul. 20, 2025); the corresponding ETAS fit is shown in Fig. 6.

We again observe $\Delta AIC \geq 2q$, favoring the two-stage model (Fig. 5). The 68% confidence interval for the change point (blue band) is $T_c=4,077-4,218$ days—Mar. 1, 2025 to Jul. 20, 2025 in days since Jan. 1, 2014. The maximum ΔAIC occurs at $T_c=4,218$ days (Jul. 20, 2025), indicating that the most probable onset of activation coincides with the $M7.4$ foreshock.

Using $T_c=4,218$ days, we fitted a single-stage ETAS model to events from Jan. 1, 2014 up to, but not including, the $M8.8$ mainshock (Fig. 6). For this fit, we set $S=0.01$ days, $T=T_c=4218$ days (July 20, 2025), and $T_{end}=4,226.49$ days (the date of the last $M \geq 5$ event before $M8.8$). During the prediction interval (after T), the observed rate (black) exceeds the extrapolated ETAS rate (red), consistent with seismic activation.

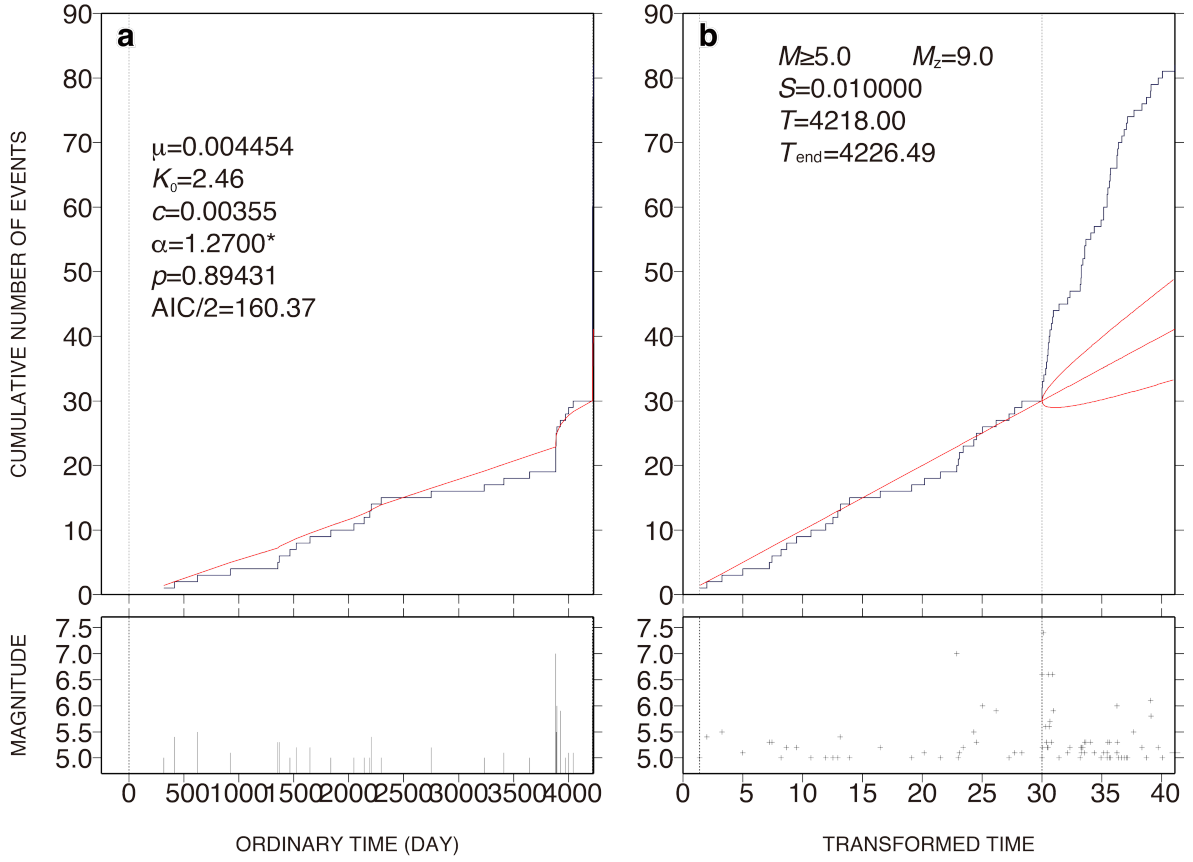


Figure 6. ETAS modeling for seismic activation (corresponding to the red-circled T_c in Fig. 5). **(a)** Cumulative counts (black) and ETAS fit (red) in ordinary time for $M \geq 5$ ($M_{\text{th}}=5$) events within a 100-km radius of the $M_{8.8}$ epicenter. Vertical dashed line marks $S=0.01$ days (Jan. 1, 2014 00:14:25) and Jul. 20, 2025 (the $M_{7.4}$ foreshock). The parameter α is fixed at 1.27. **(b)** Same as **(a)**, but in transformed time. The interval after $T=4,218$ days (Jul. 20, 2025 00:00:00) is the prediction period ($T-T_{\text{end}}$), where $T_{\text{end}}=4,226.49$ days (Jul. 28, 2025 11:45:04, the last event before the $M_{8.8}$ earthquake). The observed curve exceeds the ETAS extrapolation, consistent with seismic activation.

5 Discussion and Conclusions

The 2025 $M_{8.8}$ Kamchatka earthquake offers a unique opportunity to examine the temporal evolution of seismicity preceding a great subduction event. Using ETAS modeling and

change-point analysis (Ogata & Tsuruoka, 2016; Kumazawa et al., 2010, 2019; Nanjo et al., 2023, 2025a,b), we identified two distinct phases within a 100-km radius of the mainshock epicenter: a long-term period of seismic quiescence that began around mid-2003 and persisted for roughly two decades (Figs. 2–4), followed by a short-term activation that commenced with the *M*7.4 earthquake on 20 Jul. 2025 (Figs. 2, 5, and 6). This sequence—from prolonged quiescence to abrupt activation—mirrors patterns documented for several megathrust earthquakes, including the 1997 *M*7.8 Kronotsky, Kamchatka event (Soloviev, 2011, 2020), the 2004 *M*9.0 Sumatra event (e.g., Mignan et al., 2006; Soloviev & Lyubushin, 2007; Imoto & Yamamoto, 2008; Katsumata, 2015; Soloviev, 2020), the 2006 *M*8.3 Simushirskoe, Kuril event (Soloviev, 2011, 2020; Katsumata & Zhuang, 2020), the 2010 *M*6.4 Jiashian, Taiwan earthquake (Wen et al., 2016), and the 2011 Tohoku event (e.g., Katsumata, 2011, 2017; Kato et al., 2012; Nanjo et al., 2012; Nagao et al., 2014; Ogata, 2016). The 2025 Kamchatka case is distinguished by the clarity of its temporal transitions, the spatial confinement of activity, and the availability of continuous data spanning more than five decades.

The nearly 20-year quiescent interval revealed by the ETAS analysis is commonly interpreted as reflecting stress accumulation along a locked plate interface or evolving physical properties within the fault zone (Scholz, 2019; Mignan, 2012). Laboratory friction experiments and numerical simulations indicate that a progressive decrease in microseismicity under sustained loading can be induced by asperity healing/strengthening (Braun & Peyrard, 2018) and stress corrosion (Main & Meredith, 1991). The observed quiescence therefore likely marks a stage of interseismic stress buildup on the subduction interface beneath eastern Kamchatka.

The subsequent activation phase began about 10 days before the mainshock, coincident with the *M*7.4 event. The rapid increase in the observed rate relative to the ETAS-extrapolated rate (λ) suggests that the *M*7.4 shock may have locally increased Coulomb stress (e.g., Lin et al., 2024; Toda et al., 2025) on the locked patch that later ruptured as the *M*8.8 mainshock. Similar short-term accelerations prior to large earthquakes have been attributed to dynamic triggering, fluid-pressure transients, or aseismic-slip migration (e.g., Kato et al., 2012; Uchida & Matsuzawa, 2013; Zi et al., 2025; Peng & Lei, 2025). In Kamchatka, the sharp transition from

long-term quiescence to abrupt activation may represent the final bridge between the interseismic and coseismic phases of the earthquake cycle.

A noteworthy aspect is the separation of temporal scales between the two phases. Multi-decadal quiescence reflects slow, large-scale stress accumulation, whereas the days-long activation reflects rapid, small-scale perturbations that may ultimately trigger rupture. This hierarchical behavior implies multiple interacting timescales—from decades-long loading to transients operating over days or hours. Recognizing and quantifying both regimes are essential for improving time-dependent earthquake-probability models. Integrating long-term quiescence as a proxy for stress accumulation and short-term activation as a precursory acceleration could yield a richer probabilistic framework for assessing the imminence of large earthquakes.

Soloviev (2011, 2020), using the RTL model, found that both the *M*7.8 Kamchatka earthquake of Dec. 5, 1997 (Bourgeois & Pinegina, 2018) and the *M*8.3 Simushirskoe earthquake of Nov. 15, 2006 (Katsumata & Zhuang, 2020) along the Kuril Arc (Fig. 1b,c) exhibited a temporal sequence from quiescence to activation. Prior to the 1997 event, quiescence developed in 1994–1995, followed by activation in 1995–1996, then a return to background levels. Before the 2006 event, quiescence occurred in 2001–2003, followed by activation in 2003–2005, again returning to the background. The 1997 event ruptured a region north of the 2025 mainshock, whereas the 2006 event occurred to its south (Fig. 1b,c).

The general sequence of quiescence followed by activation in these two cases is consistent with what we identified for 2025, suggesting that heightened seismicity after a quiescent phase is a recurring characteristic of the Kamchatka–Kuril subduction system. Two differences are notable. First, the activation zone preceding the 2006 event was slightly offset from the eventual hypocenter (Soloviev, 2020), while in the 1997 and 2025 cases, the hypocenters overlapped with both the quiescent and activation areas. Second, for 1997 and 2006, there was a delay between the end of activation and the mainshock (Soloviev, 2020), whereas no such delay is evident in 2025.

Our findings underscore the value of high-resolution, long-duration seismic monitoring. Applying ETAS to multi-decadal catalogs enables quantitative detection of subtle changes in the seismicity rate (λ). The change point centered on Jun. 23, 2003 (68% confidence interval; Fig. 3), together with the statistically significant deviation of the observed rate from the ETAS-extrapolated rate (approximately 95% confidence; Fig. 4), indicates that quiescence is not merely a visual impression but a quantifiable anomaly. Similarly, the change point (Jul. 20, 2025 within 68% confidence interval; Fig. 5), together with the statistically significant deviation (above 95% confidence; Fig. 6), indicates that activation is a quantifiable anomaly. Such diagnostics could become core components of real-time forecasting when coupled with Bayesian or machine-learning frameworks that assimilate continuous data streams.

More broadly, the Kamchatka 2025 sequence reinforces that the earthquake cycle evolves dynamically rather than stationarily. Long-term quiescence likely corresponds to strain/stress accumulation, whereas short-term activation reflects the final destabilization of the fault system. Monitoring transitions between these states may improve probabilistic assessments of a large-event likelihood, especially in the Kamchatka subduction zone, and support more adaptive, transparent hazard communication. Importantly, the presence of quiescence followed by activation does not imply deterministic prediction; rather, it enhances situational awareness of evolving seismic regimes.

Limitations must be acknowledged. First, the ETAS framework assumes (piecewise) stationary parameters, whereas real fault systems may exhibit slow temporal evolution in θ due to external forcing (e.g., fluid flux or viscoelastic relaxation). Second, although the temporal coincidence between the activation onset and the *M*7.4 event is striking, causality remains to be tested with stress-transfer (e.g., Lin et al., 2024; Toda et al., 2025) and geodetic modeling. Future work should integrate high-resolution moment tensors and continuous geodetic observations to better constrain the spatiotemporal evolution of stress and coupling prior to the mainshock.

Acknowledgments. Research by K.Z.N. was partially supported by Japan's Ministry of Education, Culture, Sports, Science and Technology (MEXT) under the Second Earthquake and

Volcano Hazards Observation and Research Program (Earthquake and Volcano Hazard Reduction Research), and under the STAR-E (Seismology TowArD Research innovation with data of Earthquake) Program, Grant Number JPJ010217; the Takahashi Industrial and Economic Research Foundation (FY2025 Research Grant); and the SECOM Science and Technology Foundation (FY2023 Special Research Grant). Research by J.B.R. was supported in part by the Southern California Earthquake Center (SCEC) under grant no. SCON-00007927 to UC Davis, and by the John LaBrecque Fund, a generous gift to the University of California, Davis. SCEC Contribution Number 14988.

Open Research. The code that can be used to reproduce the results of this paper is available upon reasonable request. Data for this paper were downloaded from the USGS earthquake catalog (USGS, 2017), and are freely available at <https://earthquake.usgs.gov/earthquakes/search/>. The Generic Mapping Tools (GMT), used for Fig. 1, are an open-source collection (<https://www.generic-mapping-tools.org>). Digital model of plate boundaries (Bird, 2003), used for Fig. 1, is obtained from <https://www.earthbyte.org/category/resources/data-models/plate-boundaries/>. ETOPO Global Relief Model, that integrates topography, bathymetry, and shoreline data, used for Fig. 1, is obtained from <https://www.ncei.noaa.gov/products/etopo-global-relief-model>.

Conflict of Interest Disclosure. The authors declare there are no conflicts of interest for this manuscript.

CRedit. Conceptualization (K.Z.N., J.T., I.T.B, J.B.R.), Data curation (K.Z.N.), Formal analysis (K.Z.N.), Funding acquisition (K.Z.N., J.B.R.), Investigation (K.Z.N., J.T.), Methodology (K.Z.N., J.T., I.T.B), Project administration (K.Z.N.), Resources (K.Z.N.), Software (K.Z.N.), Supervision (K.Z.N., J.B.R.), Validation (K.Z.N.), Visualization (K.Z.N.), Writing – original draft (K.Z.N.), Writing – review & editing (K.Z.N., J.T., I.T.B, J.B.R.).

References

Akaike, H. (1974), A new look at the statistical model identification. *IEEE Transactions on Automatic Control*, 19(6), 716–723. <https://doi.org/10.1109/TAC.1974.1100705>

- Bird, P. (2003), An updated digital model of plate boundaries. *Geochemistry Geophysics Geosystems*, 4(3), 1027, <https://doi.org/10.1029/2001GC000252>.
- Bourgeois, J., Pinegina, T. K., (2018), The 1997 Kronotsky earthquake and tsunami and their predecessors, Kamchatka, Russia, *Natural Hazards and Earth System Sciences*, 18, 335–350. <https://doi.org/10.5194/nhess-18-335-2018>
- Braun, O. M., Peyrard, M. (2018), Seismic quiescence in a frictional earthquake model. *Geophysical Journal International*, 213(1), 676–683. <https://doi.org/10.1093/gji/ggy008>
- Dieterich, J. (1994), A constitutive law for rate of earthquake production and its application to earthquake clustering. *Journal of Geophysical Research*, 99(B2), 2601–2618. <https://doi.org/10.1029/93JB02581>
- Imoto, M., Yamamoto, N. (2008), Premonitory changes in seismicity prior to the Great Sumatra-Andaman earthquake of December 26, 2004. *Earth, Planets and Space*, 60, 693–697. <https://doi.org/10.1186/BF03353132>
- Inouye, W. (1965), On the seismicity in the epicentral region and its neighborhood before the Niigata earthquake. *Kenshin-jiho (Quarterly Journal of Seismology)*, 29, 139–144 (in Japanese)
- Kanamori, H. (1981), The nature of seismicity patterns before large earthquakes. In Simpson, D. W., Richards, P. G. (Eds) *Earthquake Prediction (Maurice Ewing Series 4)* (pp 1–19). American Geophysical Union, Washington D. C.
- Kato, A., Obara, K., Igarashi, T., Tsuruoka, H., Nakagawa, S., Hirata, N. (2012), Propagation of slow slip leading up to the 2011 M_w 9.0 Tohoku-oki earthquake. *Science*, 335(6069), 705–708. <https://doi.org/10.1126/science.1215141>
- Katsumata, K. (2011), A long-term seismic quiescence started 23 years before the 2011 off the Pacific coast of Tohoku Earthquake ($M = 9.0$). *Earth, Planets and Space*, 63, 709–712. <https://doi.org/10.5047/eps.2011.06.033>

- Katsumata, K. (2015), A long-term seismic quiescence before the 2004 Sumatra (M_w 9.1) earthquake. *Bulletin of the Seismological Society of America*, 105(1), 167–176.
<https://doi.org/10.1785/0120140116>
- Katsumata, K. (2017), Long-Term Seismic Quiescences and Great Earthquakes in and Around the Japan Subduction Zone Between 1975 and 2012. *Pure and Applied Geophysics*, 174, 2427–2442. <https://doi.org/10.1007/s00024-016-1415-8>
- Katsumata, K., Nakatani, M. (2021), Testing the seismic quiescence hypothesis through retrospective trials of alarm-based earthquake prediction in the Kurile–Japan subduction zone. *Earth, Planets and Space*, 73, 100. <https://doi.org/10.1186/s40623-021-01418-z>
- Katsumata, K., Zhuang, J. (2020), A new method for imaging seismic quiescence and its application to the $M_w = 8.3$ Kurile Islands earthquake on 15 November 2006. *Pure and Applied Geophysics*, 177, 3619–3630. <https://doi.org/10.1007/s00024-020-02498-w>
- Kumazawa, T., Ogata, Y., Toda, S. (2010), Precursory seismic anomalies and transient crustal deformation prior to the 2008 $M_w = 6.9$ Iwate-Miyagi Nairiku, Japan, earthquake. *Journal of Geophysical Research*, 115, B10312. <https://doi.org/10.1029/2010JB007567>
- Kumazawa, T., Ogata, Y., Tsuruoka, H. (2019), Characteristics of seismic activity before and after the 2018 $M_6.7$ Hokkaido Eastern Iburi earthquake. *Earth, Planets and Space*, 71, 130. [10.1186/s40623-019-1102-y](https://doi.org/10.1186/s40623-019-1102-y)
- Lin, J., Stein, R. S. (2004), Stress triggering in thrust and subduction earthquakes, and stress interaction between the southern San Andreas and nearby thrust and strike-slip faults. *Journal of Geophysical Research*, 109, B02303. <https://doi.org/10.1029/2003JB002607>
- Maeda, K., Hirose, F., Kobayashi, A. (2013), Precursory phenomena observed before the 2011 off the Pacific coast of Tohoku Earthquake. *Report of the Coordinating Committee for Earthquake Prediction, Japan*, 90, 503-508,
https://cais.gsi.go.jp/YOCHIREN/report/kaihou90/12_06.pdf (in Japanese)

- Main, I. G., Meredith, P. G. (1991), Stress corrosion constitutive laws as a possible mechanism of intermediate-term and short-term seismic quiescence. *Geophysical Journal International*, 107(2), 363-372. <https://doi.org/10.1111/j.1365-246X.1991.tb00831.x>
- Mignan, A. (2012), Seismicity precursors to large earthquakes unified in a stress accumulation framework. *Journal of Geophysical Research*, 39(21). L21308. <https://doi.org/10.1029/2012GL053946>
- Mignan, A., King, G., Bowman, D., Lacassin, R., Dmowska, R. (2006), Seismic activity in the Sumatra-Java region prior to the December 26, 2004 ($M_w = 9.0-9.3$) and March 28, 2005 ($M_w = 8.7$) earthquakes. *Earth and Planetary Science Letters*, 244(3-4), 639-654. <https://doi.org/10.1016/j.epsl.2006.01.058>
- Mogi, K. (1969) Some features of recent seismic activity in and near Japan (2), Activity before and after great earthquakes. *Bulletin of the Earthquake Research Institute, The University of Tokyo*, 47, 395-417
- Nagao, T., Orihara, Y., Kamogawa, M. (2014), Precursory Phenomena Possibly Related to the 2011 M9.0 Off the Pacific Coast of Tohoku Earthquake. *Journal of Disaster Research*, 9(3), 303-310. doi: 10.20965/jdr.2014.p0303
- Nagao, T., Takeuchi, A., Nakamura, K. (2011), A new algorithm for the detection of seismic quiescence: introduction of the RTM algorithm, a modified RTL algorithm. *Earth, Planets and Space*, 63, 315-324. <https://doi.org/10.5047/eps.2010.12.007>
- Nanjo, K. Z., Hirata, N., Obara, K., Kasahara, K. (2012), Decade-scale decrease in b value prior to the M9-class 2011 Tohoku and 2004 Sumatra quakes. *Geophysical Research Letters*, 39, L20304. <https://doi.org/10.1029/2012GL052997>
- Nanjo, K. Z., Kumazawa, T., Izutsu, J., Hori, T., Nagao, T., Oike, K. (2025a), Seismicity Before and After the 2023 M7.7 and M7.5 Turkey Quakes. *Geosciences*, 15(4), 113. <https://doi.org/10.3390/geosciences15040113>

- Nanjo, K. Z., Yukutake, Y., Kumazawa, T. (2023), Activated volcanism of Mount Fuji by the 2011 Japanese large earthquakes. *Scientific Reports*, 13, 10562. <https://doi.org/10.1038/s41598-023-37735-4>
- Nanjo, K. Z., Yukutake, Y., Kumazawa, T. (2025b), Changes in seismicity in a volcanically active region of the Izu Peninsula, Japan. *Journal of Volcanology and Geothermal Research*, 465, 108355. <https://doi.org/10.1016/j.jvolgeores.2025.108355>
- Ogata, Y. (1992), Detection of precursory relative quiescence before great earthquakes through a statistical model. *Journal of Geophysical Research*, 97, 19845-19871. <https://doi.org/10.1029/92JB00708>
- Ogata, Y. (1999), Seismicity analysis through point-process modeling: A review. *Pure and Applied Geophysics*, 155, 471–507. <https://doi.org/10.1007/s000240050275>
- Ogata, Y. (2011), Preshock activity and quiescence for long-term seismic activity in and around Japan. *Report of the Coordinating Committee for Earthquake Prediction, Japan*, 86, 134-141. https://cais.gsi.go.jp/YOCHIREN/report/kaihou86/03_20.pdf (in Japanese)
- Ogata, Y., Tsuruoka, H. (2016), Statistical monitoring of aftershock sequences: A case study of the 2015 Mw7.8 Gorkha, Nepal, earthquake. *Earth, Planets and Space*, 68, 44. <https://doi.org/10.1186/s40623-016-0410-8>
- Ohtake, M., Matsumoto, T., Latham, G. V. (1977), Seismicity gap near Oaxaca, Southern Mexico as a probable precursor to a large earthquake. *Pure and Applied Geophysics*, 115, 375–386. <https://doi.org/10.1007/BF01637115>
- Omori, F. (1894), On the after-shocks of earthquakes. *The journal of the College of Science, Imperial University of Tokyo, Japan*, 7, 111–200.
- Peng, Z., Lei, X. (2025), Physical mechanisms of earthquake nucleation and foreshocks: Cascade triggering, aseismic slip, or fluid flows? *Earthquake Research Advances*, 5(2), 100349. <https://doi.org/10.1016/j.eqrea.2024.100349>
- Scholz, C. H. (2019), *The Mechanics of Earthquakes and Faulting (3rd ed.)*. Cambridge University Press

- Sobolev, G. A. (2011), Seismicity dynamics and earthquake predictability. *Natural Hazards and Earth System Sciences*, 11, 445–458, <https://doi.org/10.5194/nhess-11-445-2011>
- Sobolev, G. (2020), Seismic Quiescence and Activation. In Gupta, H. (Eds) *Encyclopedia of Solid Earth Geophysics. Encyclopedia of Earth Sciences Series* (pp. 1-8). Springer, Cham. https://doi.org/10.1007/978-3-030-10475-7_185-1
- Sobolev, G. A., Lyubushin, A. A. (2007), Microseismic anomalies before the Sumatra earthquake of December 26, 2004, *Izvestiya, Physics of the Solid Earth*, 43(5), 341–353. <https://doi.org/10.1134/S1069351307050011>
- Sobolev, G. A., Tyupkin, Y. S. (1997), Low-seismicity precursors of large earthquakes in Kamchatka. *Volcanology and Seismology*, 18, 433–446.
- Toda, S., Stein, R. S., Richards-Dinger, K. & Bozkurt, S. (2005), Forecasting the evolution of seismicity in southern California: Animations built on earthquake stress transfer. *Journal of Geophysical Research*, 110, B05S16. <https://doi.org/10.1029/2004JB003415>
- Uchida, N., & Matsuzawa, T. (2013), Pre- and postseismic slow slip surrounding the 2011 Tohoku-Oki earthquake rupture. *Earth and Planetary Science Letters*, 374, 81–91. <https://doi.org/10.1016/j.epsl.2013.05.021>
- United States Geological Survey, Earthquake Hazards Program (2017), Advanced National Seismic System (ANSS) Comprehensive Catalog of Earthquake Events and Products: Various. <https://doi.org/10.5066/F7MS3QZH>.
- United States Geological Survey (2025), M8.8-2025 Kamchatka Peninsula, Russia Earthquake. <https://earthquake.usgs.gov/earthquakes/eventpage/us6000qw60/executive> (accessed on Oct. 20, 2025)
- Utsu, T. (1961), A statistical study on the occurrence of aftershocks. *Geophysics*, 30, 521–605.
- Utsu, T. (1968), Seismic activity in Hokkaido and its vicinity. *Geophysical bulletin of Hokkaido University*, 20, 51–75. <https://doi.org/10.14943/gbhu.20.51> (in Japanese)

- Wang, Q., Schoenberg, F. P., Jackson, D. D. (2010), Standard errors of parameter estimates in the ETAS model. *Bulletin of the Seismological Society of America*, 100, 1989-2001.
<https://doi.org/10.1785/0120100001>
- Wen, Y.-Y., Chen, C.-C., Wu, Y.-H., Chan, C.-H., Wang, Y.-J., Yeh, Y.-L. (2016), Spatiotemporal investigation of seismicity and Coulomb stress variations prior to the 2010 M_L 6.4 Jiashian, Taiwan earthquake. *Geophysical Research Letters*, 43(16), 8451–8457.
<https://doi.org/10.1002/2016GL070633>
- Wessel, P., Smith, W.H.F., Scharroo, R., Luis, J.F., Wobbe, F. (2013) Generic Mapping Tools: Improved version released. *Eos, Transactions American Geophysical Union*, 94(45), 409–410.
<https://doi.org/10.1002/2013EO450001>
- Wiemer, S., Wyss, M. (1994), Seismic quiescence before the Landers ($M=7.5$) and Big Bare ($M=6.5$) 1992 earthquakes. *Bulletin of the Seismological Society of America*, 84(3), 900–916.
<https://doi.org/10.1785/BSSA0840030900>
- Zi, J., Yang, Y., Yang, H. et al. (2025), The 11-month precursory fault activation of the 2019 M_L 5.6 earthquake in the Weiyuan shale gas field, China. *Communications Earth and Environment*, 6, 175. <https://doi.org/10.1038/s43247-025-02151-1>